



# **Geophysical Research Letters**

# RESEARCH LETTERDirect EUV/X-Ray Modulation of the Ionosphere During the August 2017 Total Solar Eclipse

#### **Key Points:**

- Two solar active regions caused prominent nonuniform regions inside of the penumbra at EUV/X-ray wavelengths
- The irregular EUV illumination directly modulated ionospheric electron density, producing four distinct large-scale TEC disturbances
- The 2-D manifestation of the TEC disturbances matches the 2-D projection of the EUV/X-ray irregularities

#### **Supporting Information:**

- Supporting Information S1
- Figure S1
- Movie S1
- Movie S2
- Movie S3
- Movie S4

# **Correspondence to:**

S. Mrak, smrak@bu.edu

#### Citation:

Mrak, S., Semeter, J.L., Drob, D., & Huba, J. D. (2018). Direct EUV/X-ray modulation of the ionosphere during the August 2017 total solar eclipse. *Geophysical Research Letters*, 45, 3820–3828. https://doi.org/10.1029/2017GL076771

Received 11 DEC 2017
Accepted 10 APR 2018
Accepted article online 19 APR 2018
Published online 8 MAY 2018

Sebastijan Mณี<sup>®</sup>, Joshua Seme<sup>®</sup>; Douglas Dro<sup>®</sup>, and J. **D**lubล<sup>®</sup>

<sup>1</sup>Department of Electrical and Computer Engineering and Center for Space Physics, Boston University, Boston, MA, USA, <sup>2</sup>Space Science Division, Naval Research Laboratory, Washington, Deplasma Physics Division, Naval Research Laboratory, Washington, DC, USA

**Abstract**he great American total solar eclipse of 21 August 2017 offered a fortuitous opportunity to study the response of the atmosphere and ionosphere using a myriad of ground instruments. We have used the network of U.S. Global Positioning System receivers to examine perturbations in maps of ionospheric total electron content (TEC). Coherent large-scale variations in TEC have been interpreted by others as gravity wave-induced traveling ionospheric disturbances. However, the solar disk had two active regions at that time, one near the center of the disk and one at the edge, which resulted in an irregular illumination pattern in the extreme ultraviolet (EUV)/X-ray bands. Using detailed EUV occultation maps calculated from the National Aeronautics and Space Administration Solar Dynamics Observatory Atmospheric Imaging Assembly images, we show excellent agreement between TEC perturbations and computed gradients in EUV illumination. The results strongly suggest that prominent large-scale TEC disturbances were consequences of direct EUV modulation gravity wave-induced traveling ionospheric disturbances.

Plain Language Summany solar eclipse is a rare astronomical event, which offers an opportunity to study how the Sun interacts with our atmosphere in great detail. The solar irradiance at X-ray and extreme ultra violet wavelengths is so energetic that it ionizes the neutral gases in the upper atmosphere, whereas longer wavelengths penetrate deeper in the atmosphere and heat it up. The great American total solar eclipse on 21 August 2017 offered an extraordinary opportunity to study the atmospheric response to the occulted solar disk at a time of its largest energy deposition (around noon time). The ionosphere is affected by variations in the solar illumination and by temperature changes in the lower atmosphere. We identified four large-scale perturbations in ionospheric plasma using signals acquired from a large network of Global Positioning System receivers. For the first time, we show firm evidences that irregular solar flux deposition inside of the penumbra causes a continental-wide modulation of the ionospheric plasma. Specifically, the observed disturbances were caused by two sunspots which created four stark deviations from a uniform solar disk model. The discovery of a direct solar modulation is a revolutionary turnabout, since the previous reports attributed the disturbances to thermospheric or stratospheric sources.

# 1. Introduction

A total solar eclipse is an episodic space weather event that interrupts the normal diurnal variations of the Earth's upper atmosphere and ionosphere. The direct effect in the ionosphere is a large-scale plasma depletic caused by occlusion of the EUV/X-ray source (e.g., Cohen, 1984; Coster et al., 2017; Husin et al., 2016; Momet al., 2010) with attendant effects on electrodynamic properties (e.g., St. Maurice et al., 2011). Other indirect effects include ionospheric modulation by pressure waves originating in the neutral atmosphere, known as the internal gravity waves. These waves propagate away from their source and become imprinted in the ionosphere as traveling ionospheric disturbances (TIDs), which travel at the speed of the gravity waves (typically ~30 to ~600 m/s;e.g.,Ridley et al.,1984;Roble et al.,1986).Of particular interest has been the search for stratospheric bow waves, predicted by Chimonas and Hines (1970).

These indirect effects are tingjust a few percent of the background total electron content (TEC)Yet they provide a potential diagnostic of neutral dynamics that are difficult to observe by other meants was not

©2018. American Geophysical Union. All Rights Reserved.



possible to study such perturbations until the rise of Global Positioning System (GPS) technology. GPS receive networks provide an opportunity to image the ionosphere and thus extract coherent spatial structures of tiny amplitude (e.g., Galvan et al., 2012; Grawe & Makela, 2015; Liu et al., 2011; Nykiel et al., 2017; Tsugawa et al., 2011).

The total solar eclipse of 21 August 2017 traversed North Ameripagividing an extraordinary opportunity to study the ionospheric response to altered drivers from above and below in unprecedented detaitial analyses of GPS measurements for this eclipse have revealed a total TEC reduction of 50–60% near the totality (Coster et al., 2017), as well as a variety of higher-order TEC perturbations (i.e., Coster et al., 2017; Zhang et al., 2017). As the scientific community moves forward with efforts to explain these observations, it becomes critically important to account for all possible sources.

This article describes an unexpected effect that critically impacts these efforts Jsing the reference GPS receiver network in North Americawe have filtered out the background ionosphere and the zeroth-order TEC reduction and compared maps of the TEC residuals with the extreme ultraviolet (EUV) occultation mask derived from observations by the National Aeronautics and Space Administration Solar Dynamics Observatory (SDO) spacecraft. Maps of residual perturbations closely follow irregularities in the solar EUV illumination pattern, thus providing strong evidence for direct EUV modulation of the ionosphere as their source. The findings are important due to the striking spatial similarity between some of the EUV occultation irregularities and the bow wave figure predicted by Chimonas and Hines (1970) (see TEC perturbations can be easily misinterpreted and erroneously attributed to a stratospheric physical origin.

# 2. Methodology

This study used two independent data sets. First, based on the original concepts described in Marriott et al. (1971, 1972), we used high-resolution EUV images National Aeronautics and Space Administration SDO Atmospheric Imaging Assembly (AIA) observations (Lemen et al., 2011), in conjunction with the Naval Observatory Vector Astrometry Software (Kaplan et al., 2011) software, to calculate detailed eclipse EUV occultation factors as a function of latitude, longitude, altitude, and time for this event. From the available AIA wavelength bands we chose to utilize the Fe 19.3-nm emission line as a reasonable proxy for the spatiotemporal distribution of coronal (XUV/EUV) emissions coming from the solar distributionately, it was not possible to account for the time dependence of solar XUV/EUV flux throughout the eclipse period. The SDO images were contaminated by three C-class solar flares during this time, and the SDO spacecraft was also affected by the eclipse around 19:45 UT. Therefore, the resulting mask was computed from an average of 1 hr 19.3-nm SDO AIA images between 16:00 and 17.00 UT.

An example of the eclipse computed from the AIA images and the Moon trajectory as seen from Lusk, Wyoming, is depicted in Figure 1. The AIA images reveal two active regions (blue color), one near the center and one on the very edge of the solar disk, facing the Earth. As one might expect, the active regions distort the smoothness of the Earth-projected occultation function. Figure 2a plots the computed EUV occultation factors as seen from a region of totality in Eastern Wyoming, together with a uniform disk model and the visible wavelength occultation (EUV occultation factors have been computed by inflating the actual solar disk by 15% to account for solar corona). See also Figure 2 of Huba and Drob (2017). Figure 2b shows the projection of the occultation factors as an obscuration mask on a geographical map. The contours represent lines of constant occultation factor. Overlaid is a color-coded map showing the absolute value of the second spatial derivative (Laplacian), which highlights regions of changing gradient in the EUV solar illumination. The Laplacian is commonly used in image processing as an edge detection method. The highlighted regions appear as two overlapping rings, approximately centered at the totality.

Second, we used the GPS data from stations in the continuously operating receiver station database, located between 20° and 55° GLAT, and 130° and –55° GLON, which accounts for 1,600 receivers in total. We then estimated a line-of-sight phase-corrected TEC (Coster et 1992), fit a polynomial, and then subtracted it from the estimated TEC. We have adopted a conventional TID detrending approach (e.g., Galvan et al., 2012; Haaser et al., 2017) using a 10th-order polynomial but with an important modification. The GPS-derived differential TEC has a very high amplitude resolution, that 1903 TECu (Coster et al., 2012). The high negative obscuration gradient directly in front of the totality marked as (2) in Figure 2; aused an abrupt depletion in the estimated TECA 10th-order polynomial fit would produce an oscillatory sequence of enhancement and depletion artifacts and displace the polynomial's local minimum. Since our goal is to search for coherent

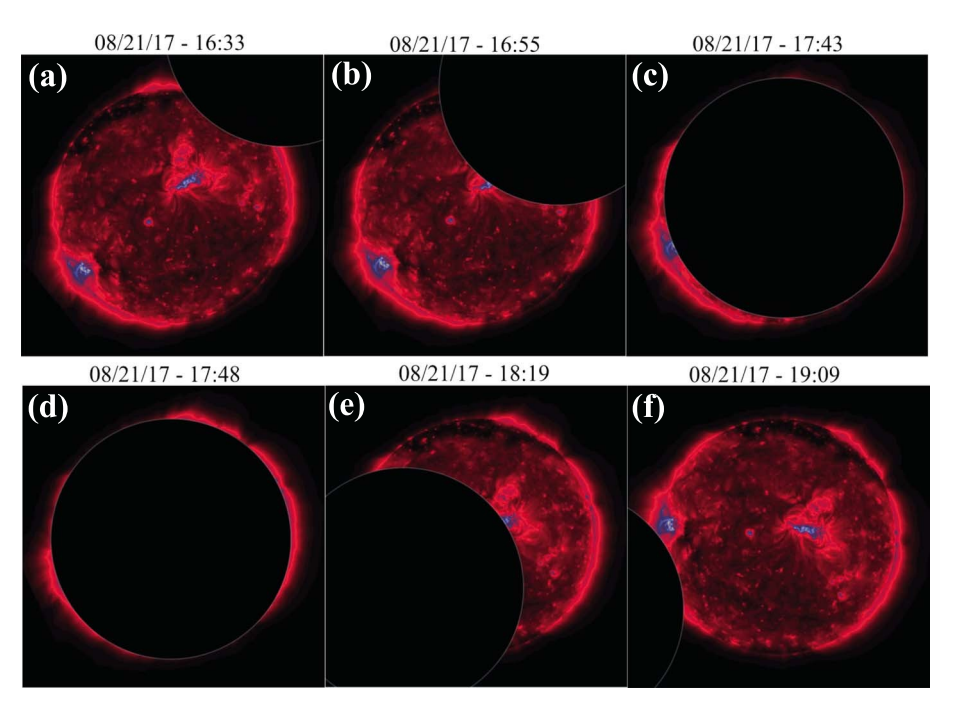


**Figure 1.** (a–f ) Solar disc surface at 19.3-nm wavelength derived from Solar Dynamics Observatory images with a calculated position of the lunar disk, as seen from Lusk, Wyoming. The Sun had two active regions on the day of the eclipse, causing a nonuniformity in the eclipse obscuration function.

small-amplitude spatial perturbations in the mapped TEC residuals, we needed to reliably remove both the normal background variations and the zeroth-order TEC depletion caused by the eclipse. We instead cut the TEC data vector for each receiver-satellite pair at the time of shortest distance from totality, creating two sepa rate vectors with a 5-min overlapping region. We then fit a polynomial of variable order (depending on vector length in time units) to each vector and subtracted itResiduals in the overlapping region were set to the mean value of the overlapping sections, suppressing possible end point effects in the polynomial fits to the data. We show example plots of the modified polynomial detrending in supporting information Figure S1. The supporting information Figure S1 shows an example of a huge deviation in the ordinary case caused by the totality, which is suppressed by the modified method. The difference between both methods away from the totality is negligible.

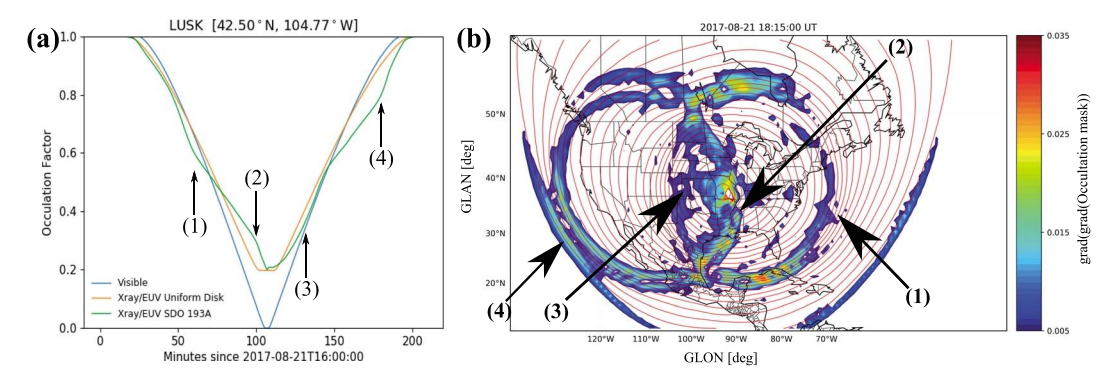


**Figure 2.** Solar extreme ultraviolet (EUV) — 19.3-nm illumination of the Earth during the eclipse, converted in to occultation factors. (a) Computed visible and XUV/EUV occultation factors at Lusk, Wyoming. (b) Spatial variations of computed EUV occultation factors at 18:15:00 UT. Contours represent regions of the same obscuration; color-coded overlay is an absolute value of the Laplacian (i.e., regions of strong gradients) of the occultation mask. Marked are four characteristic features in EUV irradiance variations, which manifested as a double ring irregular structure mapped on the geographical map.

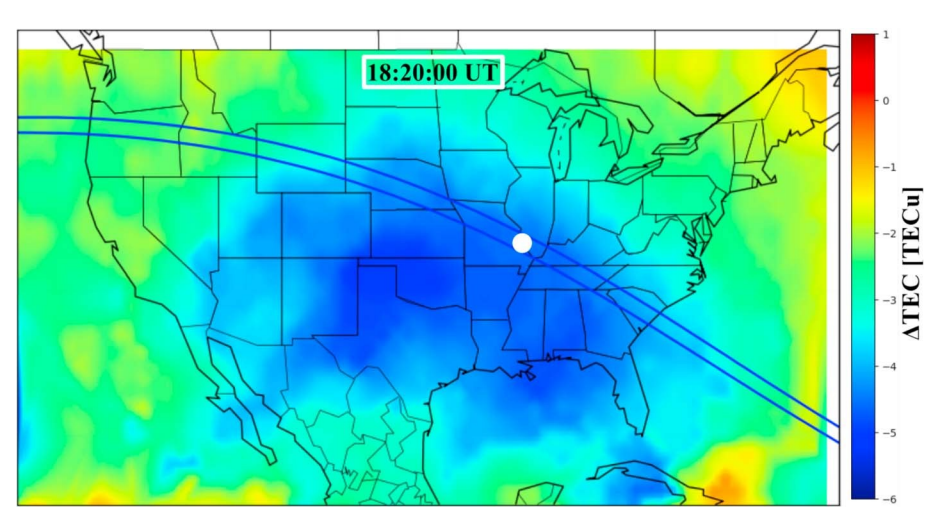


**Figure 3.** Total reduction in total electron content (TEC) due to the total solar eclipse with respect to the quiet day (day 234 — 22 August 2017). The white circle represents a position of the totality at the time of the snapshot, that is, at 18:20 UT. TEC maps were obtained via MADRIGAL Global Positioning System-TEC maps (Rideout & Coster, 2006).

# 3. Observations

Starting with a ground-projected occultation factors for Lusk, Wyoming, shown in Figure 2a, we identify four irregularities that significantly deviate from the uniform disk model. These irregularities manifest themselves as the "double ring" structure in the Laplacian of Figure 2bWe have enumerated the irregularity regions 1–4, which roughly correspond to front and back edges of double ring projection. We will refer to these four enumerated regions throughout the letter. (The transit of the occultation mask and its Laplacian over a larger field of view is included as supporting information Movie S1.)

The dominant ionospheric response to a solar eclipse is a TEC depletion due to obscuration of the ionizing EUV/X-ray source. Here we refer to this depletion the zeroth-order perturbation. The total relative TEC depletion during the eclipse is illustrated in Figure 3. The difference in absolute value of TEC was obtained by differencing the vertical TEC on the day of the eclipse (day 233, year 2017) from the day after (day 234). T TEC map was obtained using a standard MADRIGAL GPS product (Rideout & C20016), at 18:20 UTThe maximum reduction in vertical TEC at totality was TECu, and the largest depletion in TEC trails the totality point by about 30 min, which is in agreement with predictions (Huba & Drob, 2017).

The next step is to extract the TEC residuals by eliminating the background TEC, including the zeroth-order eclipse modification. In Figure 4 we show the transition of the ionospheric disturbances at the time of eclipse at 15-min cadence. Here we have used a conventional approach for imaging TEC residuals (e.g., Galvan et al 2012; Grawe & Makela, 2015; Nykiel et al., 2017; Tsugawa et al., 2011). We have mapped irregularly sampled TEC residuals onto a regular  $0.3 \cdot 0.3$  grid. The residuals are mapped at 300-km altitude—the estimated altitude of the peak in electron density at this time (Huba & Drob, 2017). Supporting information Movies S3 and S4 show the entire event presented in Figure 4 at 30-s cadence. In addition, supporting information Movies S2 shows the very same event as raw scatter plots of TEC residuals, free of any interpolation.

In Figure 4 we identify and tag the prominent large-scale TEC disturbances (1)–(4), identified in the EUV masl in Figure 2. The computed EUV Laplacian is overlaid as a contour plot. The first TEC disturbance (1), identified Figure 4a, has a crescent shape and is apparent as a faint depletion that leads the totality by 1 hr. The shape of the depletion is in excellent agreement with the EUV Laplacian prever, the relative amplitude of TEC disturbance (1) follows the intensity of the Laplacian packing its maximum over Texas. The origin of disturbance (1) can be linked back to a transition of the lunar limb over the central sunspot, depicted in Figure 1b.

The second large-scale TEC disturbance (2) is identified in Figure 4b, positioned right in front of totality. The spatial characteristics of this TEC disturbance are strikingly similar to a front wake/bow shock wayain, this prominent and stable disturbance can be related back to the EUV occultation function in Figure 2a.

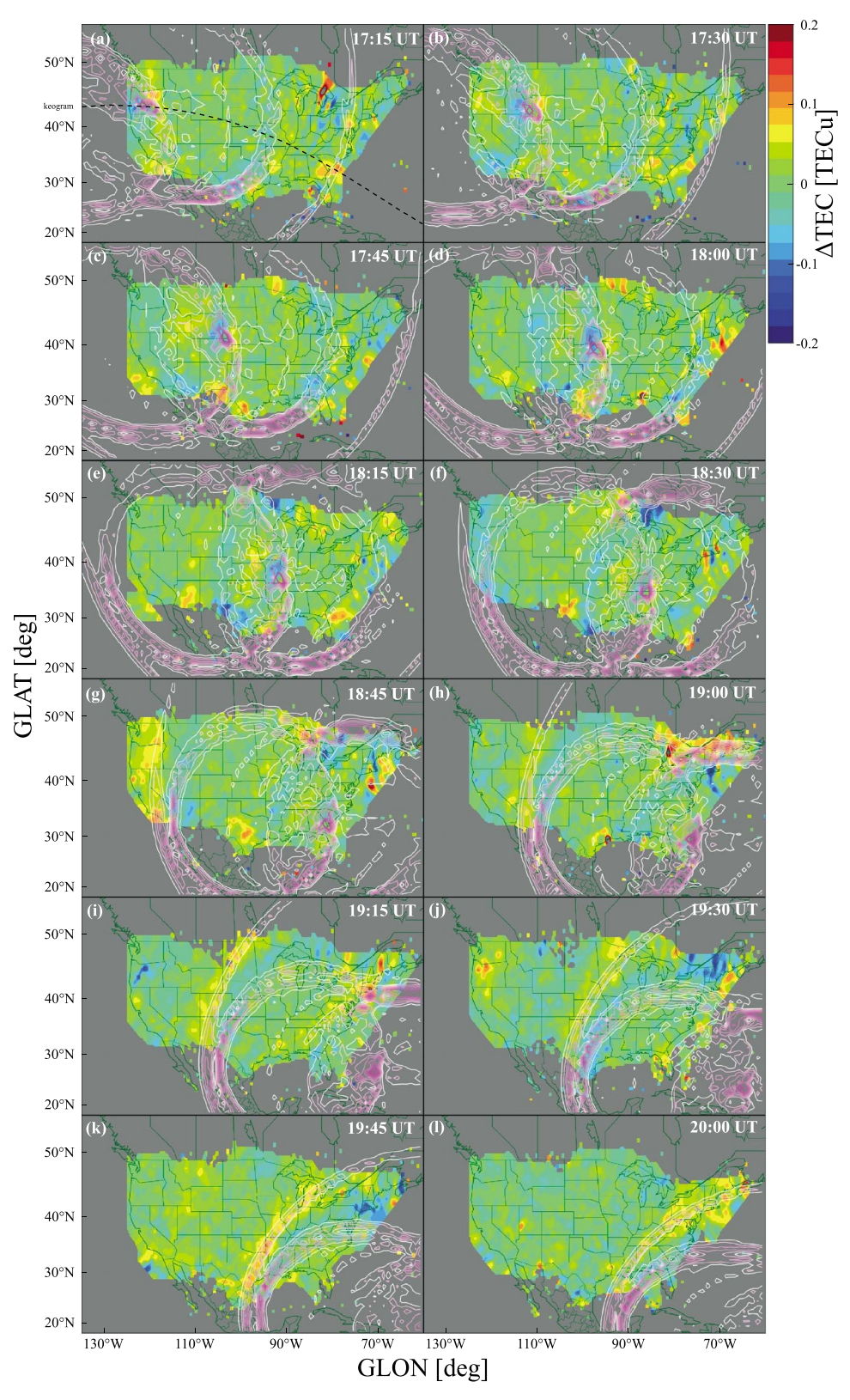


**Figure 4.** (a–l) Successive snapshots of imaged TEC residuals at 15-min cadence. Each image consists of an overplotted (contours) EUV Laplacian of the penumbra. Individual large-scale TEC disturbances (1)– (4), caused by the EUV modulation, are identified and enumerated (red). Dashed line in panel (a) depicts the center line of totality at 300 km, along which we extract the keograms in Figure 5.

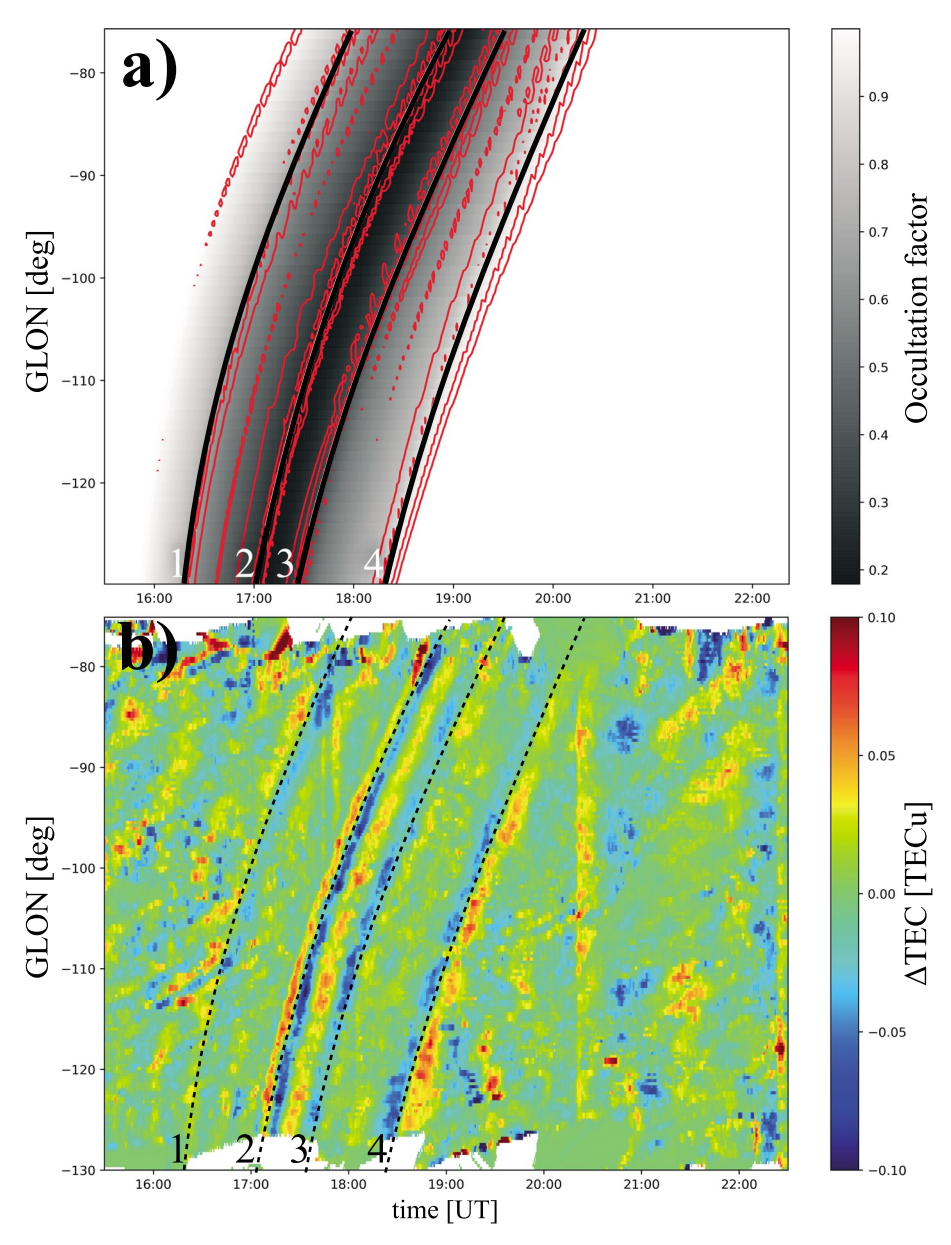


Figure 5. (a) Keogram of the obscuration mask and its Laplacian in its frame of reference. The fiducial lines are lines of maximum Laplacian. Temporal resolution is 60 s. (b) Totality-aligned keogram, averaged at 65 GLAT (dashed line in Figure 4a), for each sample in longitude. Temporal resolution is 30 s. The fiducial lines match the center (zero crossing) of all TEC disturbances, which are enumerated following the morphology established in Figure 2.

The origin of this TEC disturbance is the second sunspot, the one located on the solar limb. The bow shock-lift TEC disturbance (2) is just a manifestation of the EUV-diamond ring effect (Figure 1c) that is a sudden steep change in the ionizing source.

Similarly, we identify large-scale trailing TEC disturbances (3) and (4) in Figures 4d and 4h, respectively. The TEC disturbance (3) trails the totality \$25 min, and its shape matches the trailing edge of the first EUV ring. The origin of this disturbance can be linked back to the central sunspot at a time the lunar limb uncovered it Figure 1e. TEC perturbation (4) was a manifestation of uncovering the second sunspot on the edge of the solar disc Figure 1f. This last TEC disturbance lags the totality by about 1 hr and 30 min. The apparent shape of the latter disturbance evolved with time due to a rotation of the Sun. At earlier hours, when the projection of the disturbance (4) was located over western United States, the outer sunspot was actually the last contact of the eclipse. However, at later times, the position of the sunspot relative to the Moon moved upward,



meaning the lunar limb uncovered the sunsport earlier with respect to the eclipse phase. An example of such rotation is shown in Figure 1f. As a result the EUV modulation region split into separate regions, nicely seen in Figures 4g – 4l.

The largest gradient in EUV illumination, as presented in Figures 2b and 4 (contour overlays) was seen north and south at around 50% obscuration. These projected regions correspond to a geometry where both sunspots were located exactly on the edge of the lunar limb. This finding helps account for the relative amplitude of the TEC disturbances. The amplitudes of TEC disturbances (1) – (3) are increasing in a lateral directio away from totality slab. The relative amplitude reaches its maximum; 0.2 TECu on the very edges of our available spatial coverage.

Our findings are further emphasized through the totality-aligned (totality frame of reference) keograms in Figure 5. The TEC keogram (Figure 5b) was extracted along the line of totality, average (totality \( \frac{2}{2} \) 1.5°) in latitude for each sample in longitude In Figure 5a, the identical analysis was applied to the occultation mask (gray scale) and its Laplacian (contours). The four fiducial lines in each figure trace the maxima in the Laplacian and correspond to the four features identified in Figure 2. The eclipse-induced TEC disturbances are aligned with the lines of maximum Laplacian. The change of the tilt is a consequence of lower velocity; the entering speed was-1,000 m/s (-130° GLON), while exiting speed was about 650 m/s (GLON).

The keogram also reveals other TEC disturbances present prior to and after the eclipse. For instance, regional (northeast United States) metastable TIDs can be readily identified in Figure 4 (see also supporting information Movies) and in the keogram in Figure 5. These TIDs were present at the same location for 2 days before the confidence of the eclipse. It is thus highly unlikely that they are related to the eclipse event. Here we focus our observation and discussion solely on the four TEC disturbance features that are highly correlated with variations in the EUV occultation function.

## 4. Discussion

We break down the ionospheric response to the 21 August 2017 totalolar eclipse in to multiple orders, considering spatial scales and relative amplitudes. First, we identify the TEC depletion due to abatement of ionospheric production as the zeroth-order effect. The result shown in Figure 3 is just notional, included only to emphasize its relative amplitude and spatialextent. The eclipse-induced effects were superposed with complex space weather conditions, as discussed by Coster et al. (2017). They accounted for all space weather conditions in their analysis, including geomagnetic activity, and estimated the maximum TEC depletion to be 6–8 TECu, corresponding to 50–60% of the background TEC.

Next, we utilized polynomial detrending of the slant TEC estimates to isolate higher-order perturbations. We identified four distinct, large-scale features on a 2-D projection (Figure \*) aving a characteristic crescent/circular shape, spanning the entire north-south width of the United States, and with a relative amplitude of 0.2–0.4 TECu peak to peak the relative amplitude of the latter disturbances is of order of 3 – 7% of the zeroth-order modification; thus, we refer to them as first-order perturbations. Most of these effects have already been identified and discussed in one way or another by Coster et a(2017), Zhang et al. (2017), Nayak and Yigit (2017) and Sun et al. (2018). However, these researchers erroneously linked them to the edge of the penumbra (Zhang et al. 2017), in situ-generated thermospheric waves (Coster et a(2017), or eclipse-generated gravity waves (Nayak & Yigit, 2017; Sun et al., 2018). The perturbations are tied to the tota ity, and hence, they propagate at the same supersonic speeds correctly identified by Coster et a(2017) and Zhang et al. (2017), TIDs should travel with velocities lower than the sound speedere we have provided firm evidences (Figure 4) that these TEC perturbations are a result of a direct modulation of the ion production function due to irregular EUV illumination. Thus, we solve the puzzle of the supersonic moving TEC perturbations.

The findings presented by Nayak and Yigit (2017) and Sun et al. (2018) concern the specific TEC disturbance enumerated (2) in our Figure 2. These authors attributed this feature to an eclipse-generated gravity wave and to an acoustic shock wave, respectively. We have identified the correct physical driver for this TEC disturbance which is an active region near the edge of the solar diskThe TEC patterns associated with these sunspot occlusion events have been reported by at least four independent research groupsch using a different processing method.Thus,although the magnitude of the effect is sensitive to the detrending methodits presence is robust.



In addition, it is important to mention that our detrending method did not reveal the bow wave-like features, as found by Zhang et al. (2017). We utilized polynomial detrending, which does not involve any nonlinear operations. In contrast, Zhang et al. (2017) used a Savitzky-Goyal filter and found "V-shaped" bow wave structures trailing the totality. These bow waves would, in our images, appear between TEC features (2) and (3). Upon careful examination of the relative amplitudes of reported large-scale TEC perturbations in Zhang et al. (2017) and here (feature [4]), we notice approximately the same2 TECu relative amplitude in differential TEC. On the other hand, the bow waves found by Zhang (their Figure 2c) have a relative amplitude TECu, which corresponds to only 25% of the large-scale perturbation's amplitude. In addition, their spatial extent is significantly smaller than the EUV modulation effect. Hence, following the previously established terminology, their putative bow waves would be according to our morphology classified as second-order TEC perturbations.

It is worth noting, that we focused our observations on the continental United Statesowever, the consequences of irregular EUV illumination should be also observed in the other parts of the workstarting in central Canada where the TEC deviations should be observed by the Canadian High Arctic Ionospheric Network GPS receiversover Caribbean islands and Northern South Americand even in western Africa An accurate depiction of the regions of highly irregular EUV irradiance can be seen in the supporting information Movie S1.

# 5. Summary

Combined observations of the detrended GPS-TEC residuals and the 19.3-nm EUV occultation mask have provided firm evidences that the source of large-scale small-amplitude TEC disturbances is uneven solar EUV illumination of the Earth's atmosphere during the 2017 totalsolar eclipse. This effect is intriguing, unexpected, and potentially misleading. Namely, the shape of certain TEC irregularities (e.g., the TEC disturbance [2] in Figure 4) matches the expected morphology of atmospheric bow waves imprinted into the ionosphere. Hence, features in TEC maps may be erroneously interpreted as TIDs produced by gravity waves originating in the stratosphere (e.g., Nayak & Yigit, 2017; Sun et al., 2018).

We beak down the resulting eclipse effects on TEC into three orders of modification, regarding their statistical significance on the global atmosphere. We designate the TEC depletion as the zeroth-order modification, with a continental span and a relative amplitude of ~5 TECuNext, we mark the large-scale TEC perturbations as the first-order modification,with a spatial scale size comparing to the penumbra and with an ~0.4 TECu peal-to-peak relative amplitude. Lastly, other contemporary TEC perturbations are either regional or of a much smaller relative amplitudethus would be classified as second-order modification aggregate, we have shown that the first-order disturbances are not related to a stratospheric source. All large-scale small-amplitude disturbances may be traced to modulation of the ion production function by uneven EUV/X-ray illumination.

## **Acknowledgments**

This work was supported by the National Science Foundation under grant AGS-1743832. Work at the U.S. Naval Research Laboratory by D. Drob and J. Huba was sponsored by NASA. The differential TEC map was produced using data from the worldwide GPS receiver network MADRIGAL database, accessible on http://madrigal3. haystack.mit.edu/list/. The deternded TEC residual maps were created using data from the CORS database, publicly available on ftp://geodesy.noaa.gov/cors/. Totality track was obtained from https://eclipse.gsfc.nasa.gov/SEpath/ SEpath2001/SE2017Aug21Tpath.html.

# References

- Chimonas, G., & Hines, C. O. (1970). Atmospheric gravity waves induced by a solar eclipse. *Journal of Geophysical Research*, 75, 875. https://doi.org/10.1029/JA075i004p00875
- Cohen, E. A. (1984). The study of the effect of solar eclipses on the ionosphere based on satellite beacon observations. *Radio Science*, 19(3), 769–777. https://doi.org/10.1029/RS019i003p00769
- Coster, A. J., Goncharenko, L., Zhang, S.-R., Erickson, P. J., Rideout, W., & Vierinen, J. (2017). GNSS observations of ionospheric variations during the 21 August 2017 solar eclipse. *Geophysical Research Letters*, 44, 12,041 12,048. https://doi.org/10.1002/2017GL075774
- Coster, A. J., Gaposchkin, E. M., & Thornton, L. E. (1992). Real-time ionospheric monitoring system using GPS. *Journal of the Institute of Navigation*, 38(2), 191 204. https://doi.org/10.1002/j.2161-4296.1992.tb01874.x
- Coster, A., Herne, D., Erickson, P., & Oberoi, D. (2012). Using the Murchison Widefield Array to observe midlatitude space weather. Radio Science, 47, RS0K07. https://doi.org/10.1029/2012RS004993
- Galvan, D. A., Komjathy, A., Hickey, M. P., Stephens, P., Snively, J., Tony Song, Y., et al. (2012). Ionospheric signatures of Tohoku-Oki tsunam of March 11, 2011: Model comparisons near the epicenter. *Radio Science*, 47, RS4003. https://doi.org/10.1029/2012RS005023
- Grawe, M. A., & Makela, J. J. (2015). The ionospheric responses to the 2011 Tohoku, 2012 Haida Gwaii, and 2010 Chile tsunamis: Effects of tsunami orientation and observation geometry. Earth and Space Science, 2, 472–483. https://doi.org/10.1002/2015EA000132
- Haaser, R. A., Lay, E. H., & Junor, W. (2017). Analysis framework for systematically studying ionospheric response to impulsive events from below. *Radio Science*, 52, 1149 –1169. https://doi.org/10.1002/2016RS006196
- Huba, J. D., & Drob, D. (2017). SAMI3 prediction of the impact of the 21 August 2017 total solar eclipse on the ionosphere/plasmasphere system. *Geophysical Research Letters*, 44, 5928 5935. https://doi.org/10.1002/2017GL073549
- Husin, A., Anggarani, J. S., Ekawati, S., & Dear, V. (2016). Analysis of ionospheric irregularities during total solar eclipse 2016 based on GNSS observation. *Journal of Physics: Conference Series*, 771, 012035. https://doi.org/10.1088/1742-6596/771/1/012035
- Kaplan, G., Bartlett, J., Monet, A., Bangert, J., & Puatua, W. (2011). User's guide to NOVAS version F3.1. Washington, DC: USNO.
- Lemen, R. J., Akin, D. J., Boerner, P. F., Chou, C., Drake, J. F., Duncan, D. W., et al. (2011). The atmospheric imaging assembly (AIA) on the s dynamics observatory (SDO). *Solar Physics*, 275(1–2), 17 40. The Solar Dynamics Observatory.



# **Geophysical Research Letters**

- Liu, J. Y., Sun, Y. Y., Kakinami, Y., Chen, C. H., Lin, C. H., & Tsai, H. F. (2011). Bow and stern waves triggered by the Moon's shadow boat: SC ECLIPSE BOW AND STERN WAVES. *Geophysical Research Letters*, 38, L17109. https://doi.org/10.1029/2011GL048805
- Marriott, R. T., St. John, D. E., Thorne, R. M., & Venkateswaran, S. V. (1971). XUV image of the Sun from eclipse observations of the ionospher E-region. Solar Physics, 21(2), 483 494.
- Marriott, R. T., St. John, D. E., Thorne, R. M., Venkateswaran, S. V., & Mahadevan, P. (1972). Ionospheric effects of two recent solar eclipses. Journal of Atmospheric and Terrestrial Physics, 34(4), 695 – 712.
- Momani, M. A., Yatim, B., & Mohd Ali, M. A. (2010). Ionospheric and geomagnetic response to the total solar eclipse on 1 August 2008 over Northern Hemisphere. *Journal of Geophysical Research*, 115, A08321. https://doi.org/10.1029/2009JA014999
- Nayak, C., & Yigit, E. (2017). GPS-TEC observation of gravity waves generated in the ionosphere during 21 August 2017 total solar eclipse. Journal of Geophysical Research: Space Physics, 122, 725 – 738. https://doi.org/10.1002/2017JA024845
- Nykiel, G., Zanimonskiy, Y. M., Yampolski, Y. M., & Figurski, M. (2017). Efficient usage of dense GNSS networks in Central Europe for the visualization and investigation of ionospheric TEC variations. Sensors, 17, 2298. https://doi.org/10.3390/s17102298
- Rideout, W., & Coster, A. (2006). Automated GPS processing for global total electron content data GPS Solutions, 10, 219. https://doi.org/10.1007/s10291-006-0029-5
- Ridley, E.C., Dickinson, R.E., Roble, R.G., & Rees M. H. (1984). Thermospheric response to the June 111983, solar eclipse. Journal of Geophysical Research, 89(A9), 7583 – 7588. https://doi.org/10.1029/JA089iA09p07583
- Roble, R. G., Emery, B. A., & Ridley, E. C. (1986). Ionospheric and thermospheric response over Millstone Hill to the May 30, 1984, annular solar eclipse. *Journal of Geophysical Research*, *91*(A2), 1661 1670.
- St. Maurice, J. P., Ambili, K. M., & Choudhary, R. K. (2011). Local electrodynamics of a solar eclipse at the magnetic equator in the early afternoon hours. *Geophysical Research Letters*, 38, L04102. https://doi.org/10.1029/2010GL046085
- Sun, Y.-Y., Liu, J.-Y., Lin, C.-H., Lin, C.-Y., Shen, M.-H., Chen, C.-H., et al. (2018). lonospheric bow wave induced by the Moon shadow ship ov the continent of United States on 21 August 2017. *Geophysical Research Letters*, 45, 538 –544. https://doi.org/10.1002/2017GL075926
- Tsugawa, T., Saito, A., Otsuka, Y., Nishioka, M., Maruyama, T., Kato, H., et al. (2011). Ionospheric disturbances detected by GPS total electron content observation after the 2011 off the Pacific coast of Tohoku Earthquake. *Earth, Planets and Space*, 63(66), 875 –879. https://doi.org/10.5047/eps.2011.06.035
- Zhang, S.-R., Erickson, P. J., Goncharenko, L. P., Coster, A. J., Rideout, W., & Vierinen, J. (2017). Ionospheric bow waves and perturbations induced by the 21 August 2017 solar eclipse. *Geophysical Research Letters*, 44, 12,067 –12,073. https://doi.org/10.1002/2017GL076054